A New Semiactive Variable Stiffness Suspension System Using Combined Skyhook and Nonlinear Energy Sink-Based Controllers

Olugbenga Moses Anubi and Carl Crane

***Abstract*— This paper presents the semiactive case of a variable stiffness suspension system. The central concept is based on a recently designed variable stiffness mechanism that consists of a horizontal strut and a vertical strut, both of which are semiactively controlled by magnetorheological (MR) dampers. The vertical MR damper force is designed to track a skyhook damper force, while the horizontal strut is used is to vary the load transfer ratio by semiactively controlling the location of the point of attachment of the vertical strut to the car body. The control algorithm, effected by the horizontal MR damper, uses the concept of a nonlinear energy sink (NES) to effectively transfer the vibrational energy in the sprung mass to a control mass, thereby reducing the transfer of energy from road disturbance to the car body. The analyses and simulation results show that a better performance can be achieved by subjecting the point of attachment of a suspension system, to the chassis, to the influence of a horizontal NES system.**

***Index Terms*— Magnetorheological (MR) damper, nonlinear energy sink (NES), ride comfort, semiactive, singular perturbation, suspension, suspension deflection, variable stiffness, variance gain (VG), vehicle.**

I. Introduction

THE original concept of semiactive suspension dates back [1]–[3], where it was introduced as an alternative to the costly, highly complicated, and power-demanding active systems. While fully active suspension systems are theoretically unrestricted energy wise, semiactive elements must be either dissipative or conservative in their energy demand. So far, semiactive designs fall into a general class of variable damper, variable lever arm, and variable stiffness [4].

Variable damper type semiactive devices are capable of varying the damping coefficients across their terminals. Initial practical implementations were achieved using a variable orifice viscous damper. By closing or opening the orifice, the damping characteristics change from soft to hard and vice versa. Other methods that have been used involve the use of electrorheological (ER) or magnetorheological (MR) fluids [5]–[7]. ER and MR fluids are composed of a suspension of polarized solid particles dispersed in a nonconducting liquid. When an electric (or magnetic for MR) field is imposed, the particles become aligned along the direction of the imposed field. When this happens, the yield stress of the fluid changes, hence the damping effect. The controllable rheological properties make ER and MR fluids suitable for use as smart materials for active devices, transforming electrical energy to mechanical energy.

Variable lever arm type semiactive suspensions conserve energy between the suspension and spring storage. They are characterized by controlled force variation that consumes minimal power. The main idea behind their operation is the variation of the force transfer ratio that is achieved by moving the point of force application [8]–[12]. If this point moves orthogonally to the acting force, theoretically no mechanical work is involved in the control. This phenomenon is termed reciprocal actuation in [13].

Variable stiffness semiactive suspensions exhibit a variable stiffness feature. This is achieved either by changing the free length of a spring or by a mechanism that changes its effective stiffness characteristics as a result of one or more moving parts. In [4], an example of a hydropneumatic spring with a variable stiffness characteristic was given. In [14], a desired stiffness variation was achieved by augmenting a variable lever arm type system with a traditional passive suspension system.

Moreover, the control of semiactive suspension systems has gained a lot of research interest over the years [15]. The initial concept of suspension control also began with [1]. The initial aim of a controlled suspension was solely centered on ride comfort. One of the initial control concepts developed is the skyhook concept ([15] for an extensive description of existing skyhook-based control algorithms). A skyhook damper is a fictitious damper between the sprung mass and the inertial frame (fixed in the sky). The damping force of the skyhook damper reduces the sprung mass vibration. A similar concept called groundhook has also been developed for road friendly suspensions [16]. These control concepts have also been applied to semiactive suspensions. Other control concepts that have been applied to semiactive and active suspensions include: optimal control [17]–[20], robust control [21], robust optimal control [22]–[24], and so on.

Recently, research in semiactive suspensions has continued to advance with respect to their capabilities [15], [25]–[28], narrowing the gap between semiactive and fully active suspension systems. Meanwhile, most semiactive systems only

Manuscript received June 5, 2013; revised December 9, 2013 and June 18, 2014; accepted August 26, 2014. Date of publication September 11, 2014; date of current version April 14, 2015. Manuscript received in final form August 26, 2014. Recommended by Associate Editor S. M. Savaresi.

O. M. Anubi is with the Hyundai Center of Excellence in Vehicle System Dynamics and Control, Department of Mechanical and Aerospace Engineering, University of California at Davis, Davis, CA 95616 USA (e-mail: anubimoses@gmail.com).

C. Crane is with the Center for Intelligent Machines and Robotics, Department of Mechanical and Aerospace Engineering, University of Florida, Gainesville, FL 32611 USA (e-mail: carl.crane@gmail.com).

Color versions of one or more of the figures in this paper are available online at http://ieeexplore.ieee.org.

Digital Object Identifier 10.1109/TCST.2014.2353303

control the viscous damping coefficient of the shock absorber while keeping the stiffness constant.

On the other hand, nonlinear energy sinks (NESs) are essentially nonlinear damped oscillators that are attached to a primary system[1] for the sake of vibration absorption and mitigation. Such attachments have been used extensively in engineering applications, particularly in vibration suppression or aeroelastic instability mitigation. The vibration of systems with essential (strongly or weakly) coupled nonlinearity has been studied extensively in [29]–[33]. It was shown in [30] that such attachments can be designed to act as a sink for unwanted vibrations generated by external impulsive excitations. The underlying dynamical phenomenon governing the passive energy pumping from a primary vibrating system to the attached NES has be shown to be a resonance capture on a 1:1 manifold [33]–[38]. It was shown [37]–[39] that under certain conditions, vibration energy gets passively pumped from the directly excited primary system to the nonlinear secondary system in a one-way irreversible fashion. Nonlinear passive absorbers can be designed with far smaller additional masses than the linear absorbers [31], thanks to the energy pumping phenomenon. This corresponds to a controlled one-way channeling of the vibration energy to a passive nonlinear structure where it localizes and diminishes in time due to damping dissipation. This allows nonlinear energy pumping to be used in coupled mechanical systems, where the essential nonlinearity of the attached absorber enables it to resonate with any of the linearized modes of the substructure [33].

Recently, the concept of reciprocal actuation [13] was used to design a variable stiffness suspension (VSS) system for isolating a car body from road disturbance [40]. The system is essentially a passive vibration isolation system in which the motion of the secondary linear attachment is made orthogonal to the primary system. The primary and secondary systems are coupled through the traditional suspension system. In this paper, the above concept is extended using two semiactive devices, one controlled to mimic a skyhook damper and the other controlled to mimic a NES and used to drive the orthogonal secondary system.[2] The motivation for the use of NES is primarily due to their proven capability to achieve one-way irreversible energy pumping from the linear primary system to the nonlinear attachment. The goal therefore is to achieve a one-way irreversible energy pumping of the road disturbance to the secondary system whose vibration is orthogonal to the car body motion. A fairly general nonlinear function is used in this paper, instead of cubic nonlinearity that is generally used. Due to a few number of moving parts, the concept can easily be incorporated into existing traditional front and rear suspension designs. An implementation with a double wishbone is shown in this paper. The rest of this paper is organized as follows. In Section II, the variable stiffness concept is described, and the VSS system introduced. The control design for the MR damper is detailed in Section III. Simulation results are presented in Section V. The conclusion follows in Section VI.

[1]This refers to the main system whose vibration is intended to be absorbed.
[2]This refers to the vibration absorber or isolator.

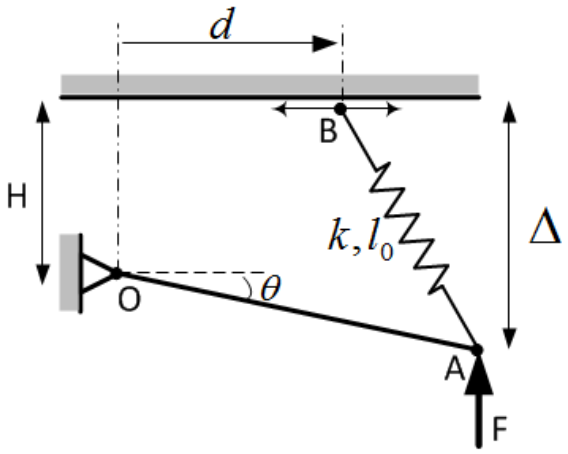

Fig. 1. Variable stiffness mechanism.

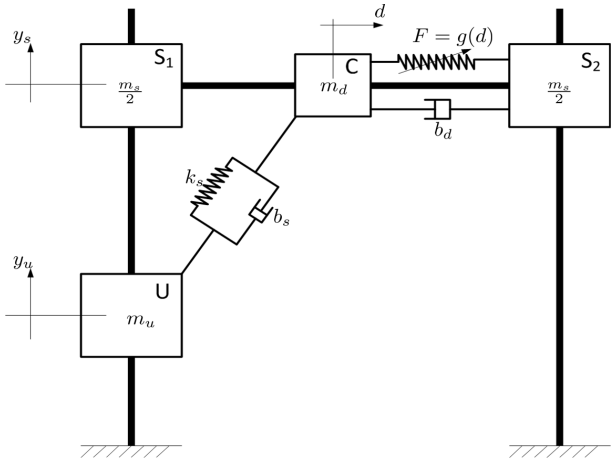

Fig. 2. Orthogonal NES.

II. System Description

This section gives a detailed description of the variable stiffness concept, the NES, and the overall suspension system.

A. Variable Stiffness Concept

The variable stiffness mechanism concept is shown in Fig. 1. The lever arm OA is pinned at a fixed point O and free to rotate about O. The spring AB is pinned to the lever arm at A and is free to rotate about A. The other end B of the spring is free to translate horizontally, as shown by the double headed arrow. Without loss of generality, the external force F is assumed to act vertically upward at point A. d is the horizontal distance of B from O. The idea is to vary the overall stiffness of the system by letting d vary actively under the influence of a horizontal linear force generator (not shown in Fig. 1). The variables k and l_0 denote the spring constant and the free length of the spring AB, respectively, and Δ the vertical displacement of the point A. The overall free length Δ_0 of the mechanism is defined as the value of Δ when no external force is acting on the mechanism.

B. Orthogonal NES

Fig. 2 shows the NES considered in this paper. The term orthogonal NES is used to describe the concept because the

TABLE I
MODEL PARAMETER VALUES

Parameter	Value
m_s	315 kg
m_u	37.5 kg
m_d	5 kg
b_s	1500 Ns/m
b_d	1500 Ns/m
b_{sky}	3000 Ns/m
k_s	29500 N/m
k_t	210000 N/m
k_1, k_d	5000 N/m
k_2	15000 N/m
l_{0_d}	0.25 m
l_{0_s}	0.5 m
A	2 cm
α_1	1

direction of motion of the secondary system is orthogonal to the primary system. This is suitable, structurally, for the application considered in this paper. The subsystems S_1, C, and S_2 constitute the primary subsystem, and are allowed to slide vertically together as a unit of total sprung mass $m_s + m_d$. The subsystem C is termed the control mass (or control subsystem). It, together with the nonlinear spring and the dashpot of damping coefficient b_d, constitutes the secondary subsystem. The nonlinear function is defined as

$$F = g(d) = -k_1(l_{0_d} - d) - k_2 \sinh(\alpha_1(l_{0_d} - d)) \quad (1)$$

where l_{0_d} is the free length of the idealized nonlinear spring. The nonlinear function used is fairly more general compared with the pure cubic nonlinearity that have been used in [41]. The Taylor series expansion is

$$F = -k_1(l_{0_d} - d) - k_2 \sum_{i=1}^{\infty} k_{2i-1}(\alpha_1)(l_{0_d} - d)^{2i-1} k_{2i-1}(\alpha_1) > 0 \quad (2)$$

from which the generality is obvious. The mass labeled U is the unsprung mass, whose displacement y_u is used as the source of disturbance to the system.

An approximate frequency response from the input y_u to the sprung mass acceleration $\ddot{y}_s$ and the rattle space deflection $y_s - y_u$ is computed using the notion of variance gain (VG) [42], [43]. The approximate VG is given by

$$G(j\omega) = \sqrt{\frac{\int_0^{2\pi N/\omega} z^2 dt}{\int_0^{2\pi N/\omega} A^2 \sin^2(\omega t) dt}} \quad (3)$$

where z denotes the performance measure of interest (sprung mass acceleration and rattle space deflection in this case). The system is excited by the sinusoid $r = A\sin(\omega t), t \in [0, 2\pi N/\omega]$, where N is an integer big enough to ensure that the system reaches a steady state. The value $N = 5$ is used in this paper. Other model parameter values used are shown in Table I. The corresponding output signals were recorded and the approximate VGs were computed using (3). The resulting VG responses are shown in Fig. 3(a) and (b)

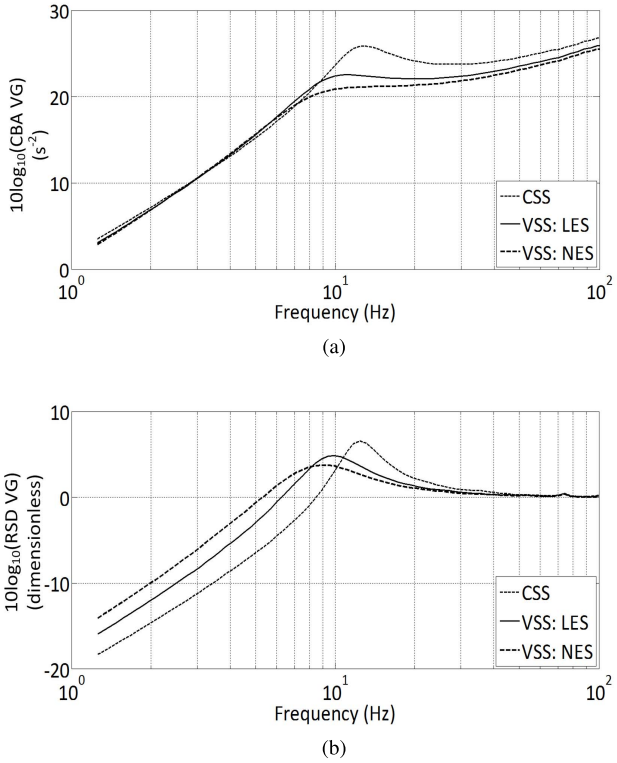

Fig. 3. VG. (a) CBA VG. (b) Rattle space displacement VG.

for the constant stiffness suspension (CSS),[3] the VSS with linear energy sink (LES),[4] and the VSS:NES. The figures show that the VSS achieves better vibration isolation, with a significant improvement from the LES case to the NES case. As shown in Fig. 3(b), the improvement gained in vibration isolation results in a corresponding performance degradation in the rattle space deflection. This observation agrees with the usual tradeoff in suspension design [24]. The performance improvement can further be increased by transitioning from LES in low-frequency range (<8 Hz) to NES in high-frequency range (>8 Hz).

C. Semiactive VSS System

The quarter car model of the suspension system considered is shown in Fig. 4. It is composed of a quarter car body, wheel assembly, two-spring-MR damper systems, road disturbance, and lower and upper wishbones. The points O, A, and B are the same, as shown in the variable stiffness mechanism in Fig. 1. The motion of the control mass, which in turn determines the effective stiffness of the suspension system, is influenced by the MR1. The MR1 damper force is designed in subsequent sections to mimic the orthogonal NES introduced in the previous section and the MR2 damper force is designed to mimic the traditional skyhook [44] damping force. The tire is modeled as a linear spring of spring constant k_t.

[3]Here, the position of the control mass is fixed. This corresponds to the traditional constant stiffness suspension system.

[4]In this case, the control mass is allowed to move under the influence of a linear horizontal spring and damper. This is the case reported in [40].

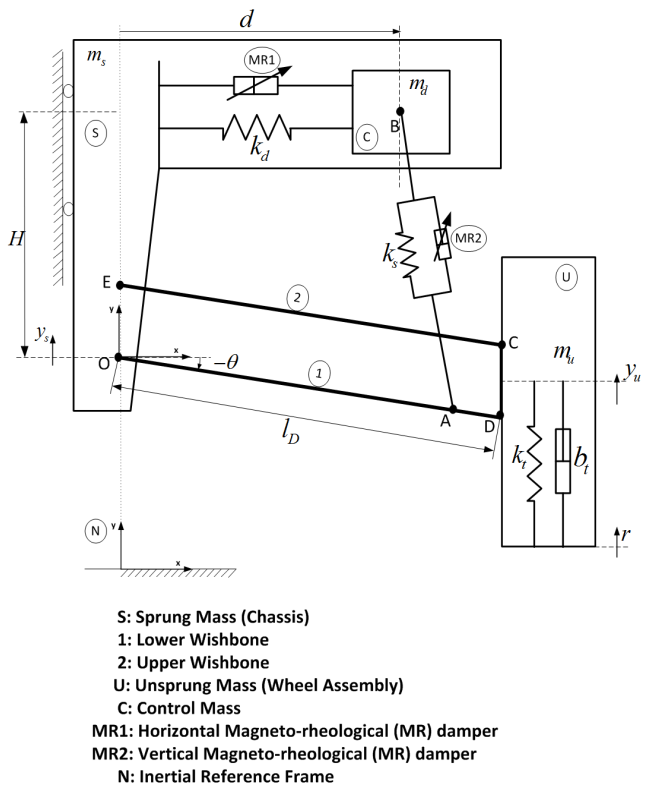

Fig. 4. Quarter car model.

The assumptions adopted in Fig. 4 are summarized as follows.

1) The lateral displacement of the sprung mass is neglected, i.e., only the vertical displacement y_s is considered.
2) The wheel camber angle is zero at the equilibrium position and its variation is negligible throughout the system trajectory.
3) The springs and tire deflections (TDs) are in the linear regions of their operating ranges.

The damping characteristics of the considered semiactive device can be changed by a control current. However, there is no corresponding energy input into the system as a result of the control current. This implies a passivity constraint on the MR-damper model. The control current is designed to mimic a desired force as close as possible, while enforcing the passivity constraint. This approach has been used in the past for semiactive control design [17], [18], [45].

D. MR-Damper Modeling

The relationship between the MR-damper control current and the damping force exhibit a nonlinear phenomenon, and as a result, MR-damper-based vibration control is a challenging task. Different damper models have been developed to capture the behavior of MR dampers. In general, the approaches that exists in the literature can be grouped into parametric and nonparametric [46], [47]. The parametric modeling technique characterizes the MR-damper device as a collection of (linear and/or nonlinear) springs, dampers, and other physical elements. A number of studies have addressed

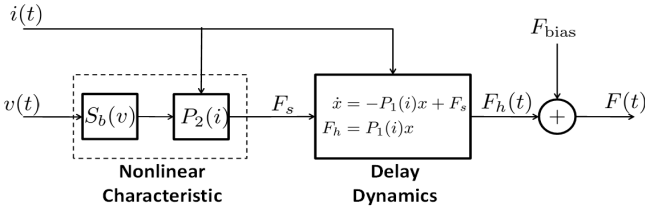

Fig. 5. Nonparametric MR-damper model.

the parametric modeling of MR dampers. One of the early models is the Bouc–Wen model [48] that was derived from a Markov-vector formulation to model nonlinear hysteric systems. Later, the Bingham viscoelastic–plastic model was described in [49]. Spencer *et al.* [5] developed a phenomenological model that accurately portrays the response of an MR damper in response to cyclic excitations. This is a modified Bouc–Wen model governed by ordinary differential equations. Bouc–Wen-based models in semiactive seismic vibration control have proven to be easy to use and numerically amenable. Other authors have studied the parametric model of MR dampers, emphasizing the difference between the preyield viscoelastic region and the postyield viscous region as a key aspect of the damper. One such model is given in [50], where the damper force is modeled using the nonlinear static semiactive damper model. This allows for fulfilling the passivity constraint of the MR damper.

On the other hand, nonparametric modeling employs analytical expressions to describe the characteristics of the modeled device based on both testing data analysis and device working principle [46]. Although parametric models effectively characterize the MR dampers at fixed values of the control current, they do not include the magnetic field saturation that is inherent in MR dampers. The representation of the magnetic field saturation is crucial in accurately using the MR-damper model for design analysis and control development. Recently, Song and Sotuhward [46] proposed a nonparametric model, where the characteristics of a commercial MR damper are represented by a series of continuous functions and differential equations, which are tractable using numerical simulation techniques. This model was used in [45] and will also be used in this paper to represent the dynamics of the MR damper. The nonparametric model is shown schematically in Fig. 5. The input to the model is the relative velocity $v(t)$ across the damper terminals, and the output is the damper force $F(t)$. The modeled aspects of the MR-damper are as follows.

1) Maximum Damping Force, $P_2(i(t))$: This is described using a polynomial function of the control current $i(t)$ as

$$P_2(i) = A_0 + A_1 i + A_2 i^2 + A_3 i^3 + A_4 i^4 \tag{4}$$

where A_j, $j = 0 - 4$ are the polynomial coefficients with appropriate units.

2) Shape Function $S_b(v(t))$: This is used to preserve the wave-shape correlation between the damper force and the relative velocity across the damper, and is given by

$$S_b(v) = \frac{(b_0 + b_1|v_r|)^{b_2 v_r} - (b_0 + b_1|v_r|)^{-b_2 v_r}}{b_0^{b_2 v_r} + b_0^{-b_2 v_r}} \tag{5}$$

TABLE II
MR-DAMPER PARAMETER VALUES

Parameter	Value	Parameter	Value	Parameter	Value
A_0	164.8	b_0	5.8646	h_2	566
A_1	1316.5	b_1	0.0060	v_0	0.6248
A_2	1407.8	b_2	0.2536	F_{bias}	0
A_3	-1562.8	h_0	299.7733		
A_4	388.8	h_1	-210.32		

where

$$v_r = v - v_0 \tag{6}$$

and $b_0 > 0, b_1 > 0, b_2 > 0$, and v_0 are constants.

3) Delay Dynamics G(s, i(t)): A first-order filter is used to create the hysteresis loop observed in experimental data. It is given in state space form as

$$\begin{aligned} \dot{x} &= -P_1(i)x + F_s = -P_1(i)x + P_2(i)S_b(v) \\ F_h &= P_1(i)x \end{aligned} \tag{7}$$

where x is the internal state of the filter and $P_1(i(t))$ is a polynomial function of the control current given by

$$P_1(i) = h_0 + h_1 i + h_2 i^2 \tag{8}$$

where h_j, $j = 0 - 2$ are polynomial coefficients with appropriate units. It is worth noting that the condition

$$P_1(i) > 0 \tag{9}$$

is imposed on $P_1(i(t))$ to guarantee a decaying solution.

4) Offset Function, F_{bias}: In some cases, the damping force is not centered at zero because of the effect of the gas-charged accumulator in the damper. The force bias F_{bias} is included in the model to capture this effect, and as result, the overall damper force is given by

$$F(t) = F_h + F_{\text{bias}}. \tag{10}$$

Table II shows the optimal values of the MR-damper model obtained from experimental data via an optimization process [46]. In terms of the input $v(t)$, (cm/s) and output $F(t)$, (N), the overall dynamics of the MR-damper is given by

$$\dot{F}_h = -P_1(i)F_h + P_1(i)S_b(v)P_2(i) \tag{11}$$

$$F(t) = F_h + F_{\text{bias}}. \tag{12}$$

III. CONTROL DEVELOPMENT

The schemes used for the desired damper forces are the NES and skyhook-based control forces

$$f_{d_H} = k_2 \dot{y}_s \sinh(\alpha_1(l_{0_d} - d)) \tag{13}$$

$$f_{d_V} = b_{\text{sky}} \dot{y}_s \tag{14}$$

where $f_{d_i}, i = \{H, V\}$ are the corresponding horizontal and vertical desired forces, respectively, k_2 and α_1 are positive constants used to tune the performance of the NES control, and b_{sky} is the damping coefficient of the skyhook damper.[5] The term $\dot{y}_s$ is used in f_{d_H} to modulate the desired horizontal damper force to make the commanded damping vanishes when the sprung mass velocity is small. This will ensure that the horizontal MR damper does not continue to remain active without road excitation.

[5]A vertical fictitious damper between the sprung mass and inertial frame.

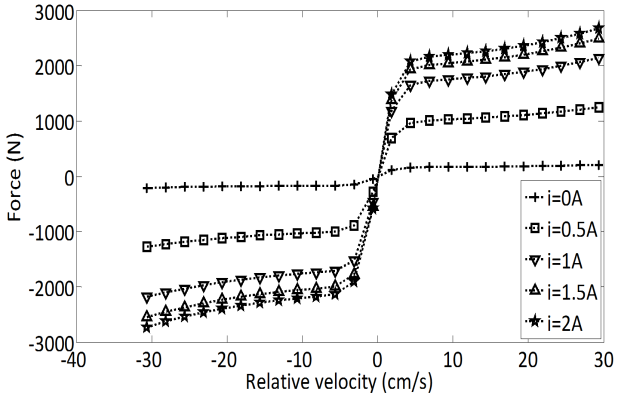

Fig. 6. Steady-state MR damper forces.

A. Open-Loop Tracking Error Development

Although the MR damper parameter values shown in Table II were determined experimentally, they can change over time due to usage and other causes. As a result, an adaptive tracking control for the MR damping force is developed. To this effect, it is assumed that the coefficients of the polynomial $P_2(i)$ are unknown. In addition, the desired control force may not generally satisfy the passivity constraint at a given instant. At the instances when the passivity constraint is violated, the desired damping force lies outside the trackable passivity region of the MR damper. To ensure a valid tracked desired damping force, the force f_{d_i} given in (13) is clipped in the passivity region. Using the final value theorem, the steady-state MR damper force, from (11), is given by

$$F_{ss} = S_b(v)P_2(i) \tag{15}$$

and Fig. 6 shows a plot of the steady-state MR damper force for different values of the input current, from which the nonlinear variation of the damper with respect to the relative velocity across the damper terminal is clearly depicted. Thus, the tracked desired damper force is obtained by clipping f_d as follows:

$$F_d(f_{d_i}, v) = \begin{cases} S_b(v)\underline{P}_2, & \text{if } v_r f_d \le v_r S_b(v)\underline{P}_2 \\ f_{d_i}, & \text{if } v_r S_b(v)\underline{P}_2 < v_r f_d < v_r S_b(v)\overline{P}_2 \\ S_b(v)\overline{P}_2, & \text{if } v_r f_d \ge v_r S_b(v)\overline{P}_2 \end{cases} \tag{16}$$

where

$$\underline{P}_2 = \min_{[0 \;\; i_{\max}]} \{P_2(i)\} \tag{17}$$

$$\overline{P}_2 = \max_{[0 \;\; i_{\max}]} \{P_2(i)\} \tag{18}$$

and $i_{\max}$ is the maximum current that can be sent to the MR damper. Now, let

$$e = F - F_d \tag{19}$$

be the tracking error of the damper force. Taking the first time derivative of (19) yields

$$\dot{e} = \dot{F} = -P_1 F + S_b P_1 P_2 \tag{20}$$
$$= -P_1(e + F_d) + S_b P_1 P_2. \tag{21}$$

The response of MR dampers are very fast compared with the vibrating mechanical system [5], [51]. Hence, the commanded desired force $F_d(\mathbf{e}, \dot{\mathbf{e}}, v)$ is assumed to be fairly constant compared to the dynamics of the MR damper. Adding and subtracting the term $P_1(-F_d + S_b\hat{P}_2)$ yields the open-loop error system

$$\dot{e} = -P_1 e + P_1 S_b(P_2 - \hat{P}_2) + P_1\alpha(i) \tag{22}$$

where

$$\alpha(i) = -F_d + S_b\hat{P}_2 \tag{23}$$

and $\hat{P}_2$ is an adaptive estimate of the polynomial $P_2(i)$. The update law is designed subsequently.

B. Closed-Loop Error System Development

First, a close approximation of the polynomial $P_2(i)$ is given within the operating interval. Given the bounds $\underline{P}_2$ and $\overline{P}_2$, the polynomial $P_2(i)$ is approximated in the interval $[0\ i_{\max}]$ as

$$P_2(i) = \underline{P}_2 + \frac{i}{i_{\max}}\left(\overline{P}_2 - \underline{P}_2\right) + \beta(i) \tag{24}$$

where

$$\beta(i) = i(i - i_{\max})(\theta_0 + i\theta_1 + i^2\theta_2) \tag{25}$$

is chosen to satisfy the constraints $\beta(0) = \beta(i_{\max}) = 0$, which implies that $P_2(0) = \underline{P}_2$ and $P_2(i_{\max}) = \overline{P}_2$. The approximation is largely dependent on the monotonicity and the onto properties of $P_2(i)$.

Lemma 1: There exists unique ideal parameters $\underline{P}_2, \overline{P}_2, \theta_0, \theta_1,$ and θ_2 such that the approximated polynomial given in (24) matches the original polynomial in (4) exactly.

Proof: The approximated polynomial is written in an expanded form as follows:

$$P_2(i) = \underline{P}_2 + i\left(\frac{\overline{P}_2 - \underline{P}_2}{i_{\max}} - \theta_0 i_{\max}\right) + i^2(\theta_0 - \theta_1 i_{\max}) + i^3(\theta_1 - \theta_2 i_{\max}) + i^4\theta_2. \tag{26}$$

Comparing (26) with (4) yields the system of linear equation

$$\begin{bmatrix} 1 & 0 & 0 & 0 & 0 \\ 1 & -1 & -i_{\max}^2 & 0 & 0 \\ 0 & 0 & 1 & -i_{\max} & 0 \\ 0 & 0 & 0 & 1 & -i_{\max} \\ 0 & 0 & 0 & 0 & 1 \end{bmatrix} \begin{bmatrix} \underline{P}_2 \\ \overline{P}_2 \\ \theta_0 \\ \theta_1 \\ \theta_2 \end{bmatrix} = \begin{bmatrix} A_0 \\ A_1 i_{\max} \\ A_2 \\ A_3 \\ A_4 \end{bmatrix}. \tag{27}$$

The determinant of the coefficient matrix in (27) is -1, which implies that the coefficient matrix is full ranked. As a result, there exists a unique vector $[\,\underline{P}_2\ \overline{P}_2\ \theta_0\ \theta_1\ \theta_2\,]^T$ that satisfies (27). □

Fig. 7 shows the plot of the actual and the approximated polynomials with θ_0, θ_1, and θ_2 determined using least square method, given $\underline{P}_2$ and $\overline{P}_2$.

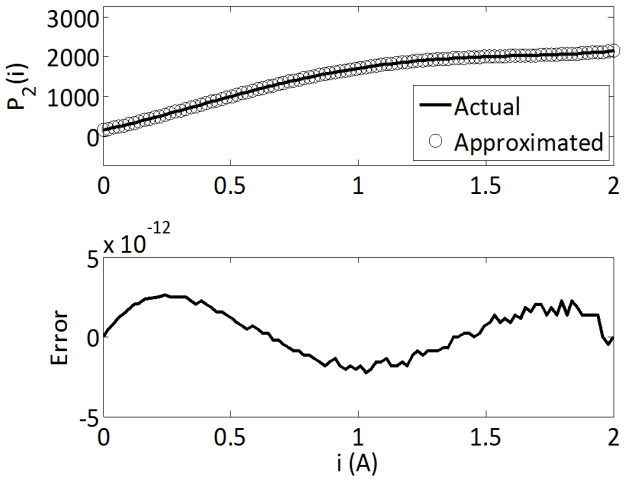

Fig. 7. Polynomial approximation.

The polynomial in (24) is linear in the unknown parameters θ_j, $j = 0 - 2$. Thus, (22) becomes

$$\dot{e} = -P_1 e + S_b P_1 Y^T(\Theta - \hat{\Theta}) + P_1\alpha(i) \tag{28}$$
$$= -P_1 e + S_b P_1 Y^T\tilde{\Theta} + P_1\alpha(i) \tag{29}$$

where

$$\Theta = [\,\theta_0\ \ \theta_1\ \ \theta_2\,]^T \tag{30}$$

is the parameter vector to be estimated, with a corresponding parameter estimation error vector

$$\tilde{\Theta} = \Theta - \hat{\Theta} \tag{31}$$

$$Y = i(i - i_{\max})\begin{bmatrix} 1 \\ i \\ i^2 \end{bmatrix}^T \tag{32}$$

is the current-dependent regression matrix, and

$$\hat{P}_2(i) = \underline{P}_2 + \frac{i}{i_{\max}}\left(\overline{P}_2 - \underline{P}_2\right) + Y(i)^T\hat{\Theta}. \tag{33}$$

The following lemma is used to guarantee the existence of a valid control current in the interval $[0\ i_{\max}]$.

Lemma 2: If the parameter update law is designed such that the estimate $\hat{\Theta}$ is continuous, then the polynomial $\alpha(i)$ given in (23) has at least one root in the operating interval $[0\ i_{\max}]$.

Proof: From (16), it is seen that the clipped desired damping force satisfies the following passivity constraint:

$$(v - v_0)S_b(v)\underline{P}_2 \le (v - v_0)F_d(u, v) \le (v - v_0)S_b(v)\overline{P}_2. \tag{34}$$

In addition, from (5), it can be shown that the term $(v - v_0)$ $S_b(v)$ is positive. Thus, dividing through by $(v - v_0)S_b(v)$ in (34) yields

$$\underline{P}_2 \le \frac{F_d(f_d, v)}{S_b(v)} \le \overline{P}_2 \tag{35}$$

which implies that

$$\frac{F_d(f_d, v)}{S_b(v)} \in \left[\underline{P}_2\overline{P}_2\right]. \tag{36}$$

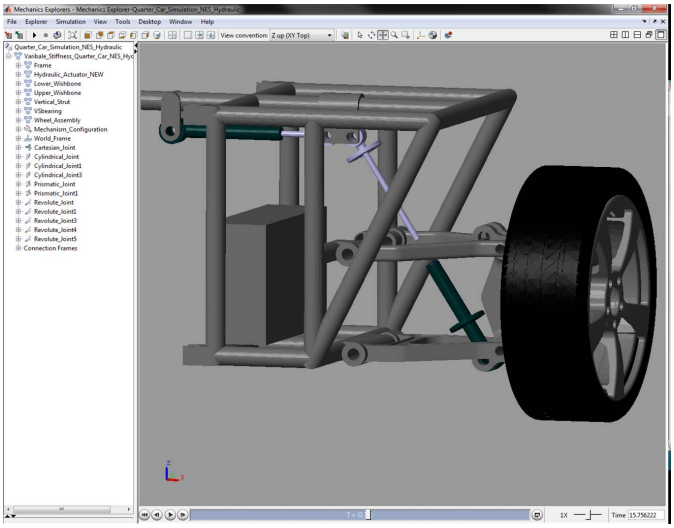

Fig. 8. SimMechanics model.

Since $\hat{\Theta}$ is continuous by the hypothesis, it implies that $\hat{P}_2(i)$ is continuous. In addition, since $\hat{P}_2(0) = \underline{P}_2$ and $\hat{P}_2(i_{\max}) = \overline{P}_2$, using the intermediate value theorem, it follows that there exists at least one $i_c \in [0\ i_{\max}]$ such that:

$$\hat{P}_2(i_c) = \frac{F_d(f_d, v)}{S_b(v)} \tag{37}$$

which implies that

$$\alpha(i_c) = F_d(f_d, v) - S_b(v)\hat{P}_2(i_c) = 0. \tag{38}$$

Thus, $i_c \in \text{roots}(\alpha(i))$, and since $i_c \in [0\ i_{\max}]$, the proof is complete. □

Next, suppose that $\hat{\Theta}$ is continuous, then, using Lemma 2, it follows that there exists a control current $i_c \in [0\ i_{\max}]$ such that $\alpha(i_c) = 0$. Consequently, the closed-loop error system is given by

$$\dot{e} = -P_1 e + S_b P_1 Y(i_c)^T \tilde{\Theta}. \tag{39}$$

IV. Stability Analysis

Theorem 1: Given the update law

$$\dot{\hat{\Theta}} = L e S_b(v) Y(i_c), \quad \Theta(0) = \Theta_0 \tag{40}$$

where L is a positive constant adaptation gain and the control law

$$i_c = \arg \min_{[0\ i_{\max}]} \text{roots}(\alpha(\tau)) \tag{41}$$

the closed-loop error dynamics in (39) is stable, and the tracking error $e(t)$ approaches zero asymptotically. In addition, the parameter estimate $\hat{\Theta}$ is continuous, thus satisfying the hypothesis of Lemma 2.

Proof: Consider the positive definite Lyapunov candidate function

$$V_L = \frac{1}{2}e^2 + \frac{1}{2}\tilde{\Theta}^T\tilde{\Theta}. \tag{42}$$

Taking the first time derivative of (42) along the closed-loop trajectory in (39) yields

$$\dot{V}_L = e\dot{e} - \tilde{\Theta}\dot{\hat{\Theta}} \tag{43}$$

$$= e(-P_1 e + S_b P_1 Y(i_c)^T \tilde{\Theta}) - \tilde{\Theta}^T \dot{\hat{\Theta}}. \tag{44}$$

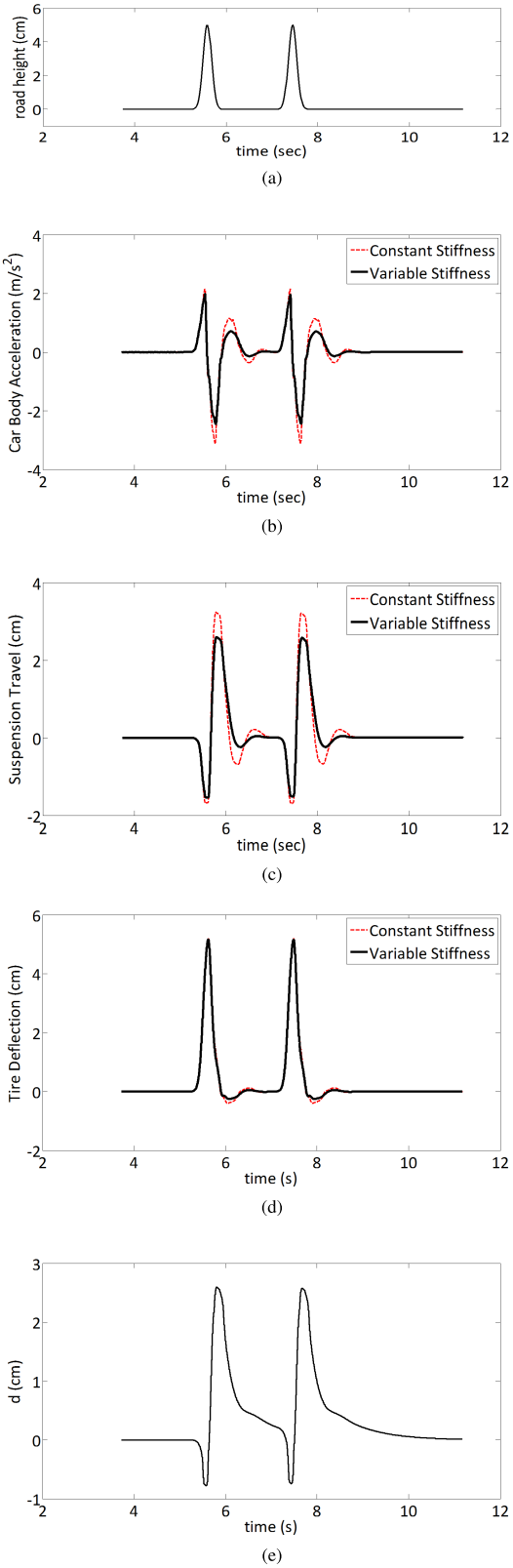

Fig. 9. Time-domain simulation: responses. (a) Road excitation profile. (b) CBA. (c) ST. (d) TD. (e) Control mass displacement.

Substituting the update law in (40) yields

$$\dot{V}_L = -P_1 e^2. \tag{45}$$

Since $P_1(i) > 0$, it implies that $\dot{V}_L$ is negative semidefinite, and since V_L is positive definite, it follows that $V_L \in \mathcal{L}_\infty$.

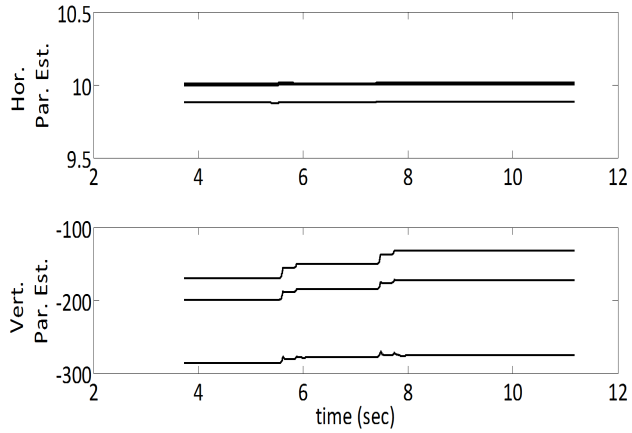

(a)

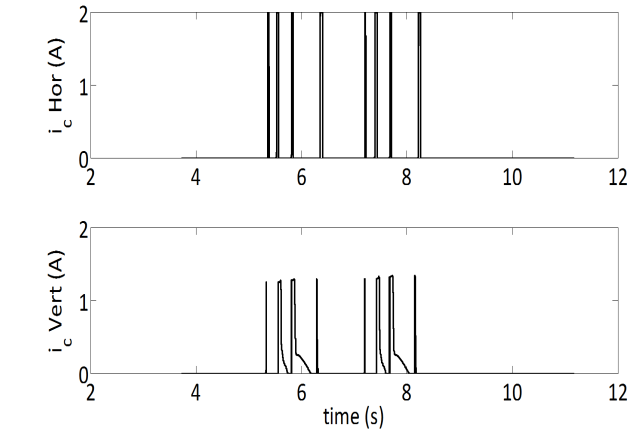

(b)

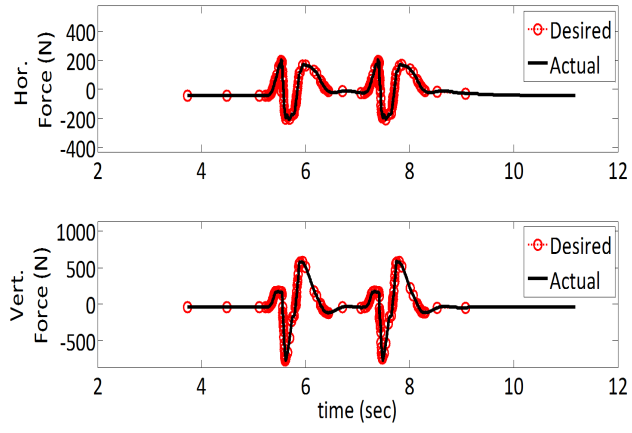

(c)

Fig. 10. Time-domain simulation: control entities. (a) Parameter estimates. (b) Control currents. (c) MR-damper forces.

From (42), it follows that $e, \tilde{\Theta} \in \mathcal{L}_\infty$, which also implies that $\hat{\Theta} \in \mathcal{L}_\infty$ since Θ is a constant. Integrating (45) yields

$$V_L - V_L(0) \leq -\int_0^t P_1(i(\tau))e(\tau)^2 d\tau \tag{46}$$

from which it follows that $e \in \mathcal{L}_2$. Also from (39), it follows that $\dot{e} \in \mathcal{L}_\infty$, which implies that e is uniformly continuous. Thus, since $e \in \mathcal{L}_2$ and is uniformly continuous, it can be shown using Barbalat's lemma [52] that $e(t) \to 0$ asymptotically. □

Algorithm 1 Control/Update $f_d, v, \hat{\Theta}$

comment: *Clipped Desired Force*

$F_d \leftarrow F_d(f_d, v)$

comment: *Compute tracking error*

$e \leftarrow F - F_d$

comment: *Compute control current*

$i_c = \min_{[0 \quad i_{max}]} roots\left(-F_d + S_b(v)\hat{P}_2(i)\right)$

comment: *Parameter Update*

$\hat{\Theta} \leftarrow L\int_0^t e(\tau)S_b(v)Y(i_c)d\tau + \hat{\Theta}_0$

return $(i_c, \hat{\Theta})$

TABLE III
VG VALUES

	Constant Stiffness	Constant Stiffness (Soft)	Variable Stiffness	Variable Stiffness (Soft)
CBA (s^{-2})	69.63	60.7	56.48	52.63
ST	0.82	0.94	0.69	0.83
TD	1.04	1.05	1.03	1.03

Remark 1: Algorithm 1 summarizes the control and update laws developed in the last two sections.

V. Simulation Results

To study the behavior of the quarter car system to different road excitation scenarios as well as measure responses like suspension deflection and realistic simulations were carried out using MATLAB SimMechanics. First, the system was modeled in Solidworks, and then translated to a SimMechanics model (Fig. 8). The vertical strut and tire damping and stiffness used are the ones given in the Renault Mégane Coupé model [53]. The values are shown in Table I.

In the simulation, the vehicle traveling at a steady horizontal speed of 40 mph is subjected to the road profile shown in Fig. 9(a). The car body acceleration (CBA), suspension travel (ST), and TD responses are measured. The ST is defined as the vertical displacement of the center of mass of the sprung mass with respect to the unsprung mass and the TD as the vertical displacement of the unsprung mass with respect to the road level. Simulations were carried out for the constant stiffness and the VSS systems. For the CSS, the control mass was locked at a fixed position corresponding to the equilibrium position of the control mass for the variable stiffness system. The results obtained are shown in Figs. 9 and 10. Table III shows the VGs for the different responses. Fig. 9(b) shows the CBA, which is used here to describe the ride comfort. The lower the CBA, the better the ride comfort. In Table III, additional VGs are reported for soft suspensions (60% of the nominal stiffness). As can be seen, the softer the suspension, the better the ride comfort for both the constant and variable stiffness cases. However, associated with this improvement is a corresponding degradation in the ST. This agrees with the well-known tradeoff between ride comfort and suspension deflection. Fig. 9(d) shows that there is no significant reduction in the TD. Thus, the suspension systems are approximately

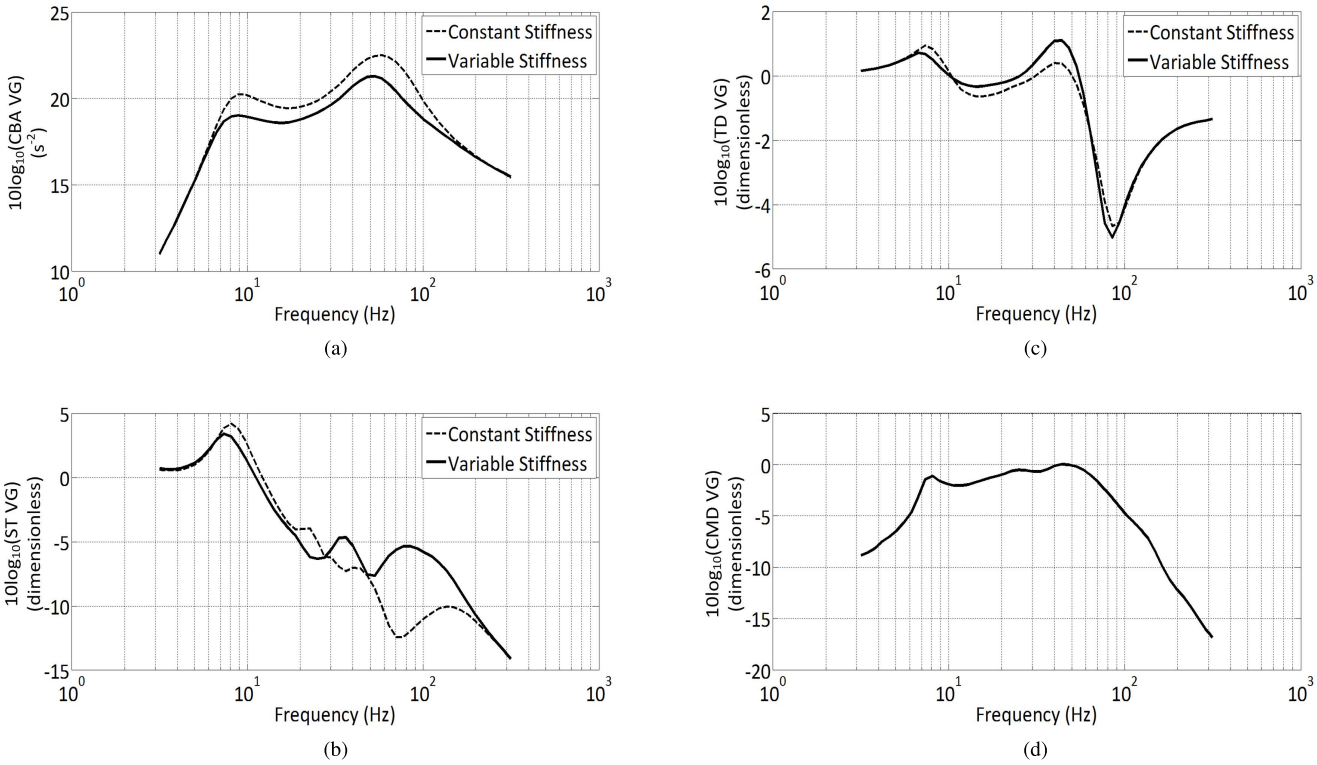

Fig. 11. VG. (a) CBA VG. (b) ST VG. (c) TD VG. (d) Control mass displacement VG.

equally road friendly. Fig. 9(e) shows the position history of the control mass for the VSS, from which the boundedness of the motion of the control mass is seen. The maximum displacement of the control mass from the equilibrium position is less than 5 cm. This implies that the space requirement for the control mass is small, which further demonstrates the practicality of the system. Fig. 10(a) shows the parameter estimates. The upper subfigure shows that the parameters are not updated in the control of the horizontal MR damper. This is because the corresponding control current is bang–bang, switching from $i_c = 0$ to $i_c = i_{\max}$. As a result, the elements of the regression matrix given in (32) are zeros, which further implies, from (40), that $\dot{\hat{\Theta}} = 0$. Thus, the parameter estimate will remain constant. Fig. 10(c) shows that the horizontal and vertical damper forces track the corresponding desired damper forces reasonably well.

Moreover, to give an in-depth evaluation of the system performance, an approximate frequency response is carried out using the notion of VG described in Section II-B. The results are reported in Fig. 11. In Fig. 11(a), it observed that the improvement in ride friendliness introduced by the variable stiffness architecture is preserved across the frequency range considered. Fig. 11(b) and (c) shows the approximate frequency response of the ST and TD, respectively. Fig. 11(d) shows the VG of the displacement of the control mass across the considered frequency range.

VI. Conclusion

The design, analysis, and control of the semiactive case of a new VSS system is presented. The vertical MR damper force is designed to track a skyhook damper force, while the horizontal MR damper control algorithm uses the concept of NES to effectively transfer the vibrational energy in the sprung mass to a control mass. Simulation results show that the new system shows a significant improvement in ride comfort over the traditional vertical skyhook controller. Associated with the ride improvement is a slight degradation in the suspension deflection performance, but the suspension limit is not exceeded. There is no significant change in the road holding performance. Thus, a better semiactive suspension performance, in terms of comfort, can be achieved using an additional semiactive device to control the horizontal location of the point of attachment of the vertical strut to the car body, and controlled to mimic a fictitious NES attached between the control mass and the vehicle body.

In the future, the effect of this VSS system on the vehicle ride height will be examined via simulation and experiment.

References

[1] D. Karnopp, M. J. Crosby, and R. A. Harwood, "Vibration control using semi-active force generators," *J. Manuf. Sci. Eng.*, vol. 96, no. 2, pp. 619–626, 1974.

[2] D. Karnopp, "Active damping in road vehicle suspension systems," *Veh. Syst. Dyn., Int. J. Veh. Mech. Mobility*, vol. 12, no. 6, pp. 291–311, 1983.

[3] D. Karnopp and G. Heess, "Electronically controllable vehicle suspensions," *Veh. Syst. Dyn., Int. J. Veh. Mech. Mobility*, vol. 20, nos. 3–4, pp. 207–217, 1991.

[4] M. Valasek and W. Kortum, "Semi-active suspension systems II," in *The Mechanical Systems Design Handbook: Modeling, Measurement, and Control*. Boca Raton, FL, USA: CRC Press, 2001.

[5] B. F. Spencer, Jr., S. J. Dyke, M. K. Sain, and J. D. Carlson, "Phenomenological model of magnetorheological damper," *ASCE J. Eng. Mech.*, vol. 123, no. 3, pp. 230–238, 1997.

[6] J. W. Kim, Y. H. Cho, H. J. Choi, H. G. Lee, and S. B. Choi, "Electrorheological semi-active damper: Polyaniline based ER system," *J. Intell. Mater. Syst. Struct.*, vol. 13, nos. 7–8, pp. 509–513, 2002.

[7] A. Ashfak, A. Saheed, K. K. Abdul-Rasheed, and J. A. Jaleel, "Design, fabrication and evaluation of MR damper," *World Acad. Sci., Eng. Technol.*, vol. 53, no. 1, pp. 27–33, 2011.

[8] O. M. Anubi and C. Crane, "Semi-global output feedback asymptotic tracking for an under-actuated variable stiffness mechanism," in *Proc. 13th IFTOMM World Congr. Mech. Mach. Sci.*, Jun. 2011.

[9] A. C. M. van der Knaap, "Design of a low power anti-roll/pitch system for a passenger car," Ph.D. dissertation, Veh. Res. Lab., Delft Univ. Technology, Delft, The Netherlands, 1989.

[10] P. J. T. Venhovens and A. C. M. van der Knaap, "Delft active suspension (DAS) background theory and physical realization," *Smart Veh.*, pp. 139–165, 1995, [Online]. Available: http://trid.trb.org/view.aspx?id=458373

[11] A. C. M. van der Knaap, A. P. Teerhuis, R. B. G. Tinsel, and R. M. A. F. Vershuren, "Active suspension assembly for a vehicle," U.S. Patent 2008 049 845, May 2, 2008.

[12] W.-J. Evers, A. Teehuis, A. van der Knaap, I. Besselink, and H. Nijmeijer, "The electromechanical low-power active suspension: Modeling, control, and prototype testing," *J. Dyn. Syst., Meas., Control*, vol. 133, pp. 041008-1–041008-9, Apr. 2011.

[13] O. M. Anubi, C. Crane, III, and S. Ridgeway, "Design and analysis of a variable stiffness mechanism," in *Proc. ASME Int. Design Eng. Tech. Conf. Comput. Inf. Eng. Conf. (IDETC/CIE)*, 2010, pp. 589–596.

[14] O. M. Anubi and C. D. Crane, III, "Nonlinear control of semi-active macpherson suspension system," in *Proc. ASME Int. Design Eng. Tech. Conf. Comput. Inf. Eng. Conf.*, 2012, pp. 397–406.

[15] S. M. Savaresi, C. Poussot-Vassal, C. Spelta, O. Sename, and L. Dugard, *Semi-Active Suspension Control Design for Vehicles*. Amsterdam, The Netherlands: Elsevier, 2010.

[16] M. Valasek and W. Kortüm, "Nonlinear control of semi-active road-friendly truck suspension," in *Proc. AVEC*, Nagoya, Japan, 1998, pp. 275–280.

[17] T. Butsuen, "The design of semi-active suspensions for automotive vehicles," Ph.D. dissertation, Dept. Mech. Eng., Massachussets Inst. Technology, Cambridge, MA, USA, 1989.

[18] H. E. Tseng and J. K. Hedrick, "Semi-active control laws—Optimal and sub-optimal," *Veh. Syst. Dyn., Int. J. Veh. Mech. Mobility*, vol. 23, no. 1, pp. 545–569, 1994.

[19] H. Tanghirad and E. Esmailzadeh, "Automobile passenger comfort assured through LQG/LQR active suspension," *J. Vibrat. Control*, vol. 4, no. 5, pp. 603–618, 1998.

[20] E. Elbeheiry, D. Karnopp, and A. Abdelraaouf, "Suboptimal control design of active and passive suspensions based on a full car model," *Veh. Syst. Dyn., Int. J. Veh. Mech. Mobility*, vol. 26, no. 3, pp. 197–222, 1996.

[21] F. Lin, *Robust Control Design: An Optimal Control Approach*. West Sussex, U.K.: Wiley, 2007.

[22] E. Ono, S. Hosoe, H. D. Tuan, and Y. Hayashi, "Nonlinear h_∞ control of active suspension," *Veh. Syst. Dyn. Supplement*, vol. S1, pp. 489–501, 1996.

[23] A.-L. Do, O. Sename, and L. Dugard, "An LPV control approach for semi-active suspension control with actuator constraints," in *Proc. Amer. Control Conf.*, 2010, pp. 4653–4658.

[24] I. Fialho and G. J. Balas, "Road adaptive active suspension design using linear parameter-varying gain-scheduling," *IEEE Trans. Control Syst. Technol.*, vol. 10, no. 1, pp. 43–54, Jan. 2002.

[25] E. R. Wang, X. Q. Ma, S. Rakheja, and C.-Y. Su, "Semi-active control of vehicle vibration with MR-dampers," in *Proc. 42nd IEEE Conf. Decision Control*, vol. 3. Dec. 2003, pp. 2270–2275.

[26] S. M. Savaresi and C. Spelta, "A single-sensor control strategy for semi-active suspensions," *IEEE Trans. Control Syst. Technol.*, vol. 17, no. 1, pp. 143–152, Jan. 2009.

[27] O. M. Anubi, C. D. Crane, III, and W. E. Dixon, "Nonlinear disturbance rejection for semi-active MacPherson suspension system," in *Proc. ASME 5th Annu. Dyn. Syst. Control Conf.*, Fort Lauderdale, FL, USA, 2012, pp. 513–522.

[28] C. Spelta *et al.*, "Performance analysis of semi-active suspensions with control of variable damping and stiffness," *Veh. Syst. Dyn., Int. J. Veh. Mech. Mobility*, vol. 49, nos. 1–2, pp. 237–256, 2011.

[29] Y. Starosvetsky and O. V. Gendelman, "Vibration absorption in systems with a nonlinear energy sink: Nonlinear damping," *J. Sound Vibrat.*, vol. 324, nos. 3–5, pp. 916–939, 2009.

[30] A. F. Vakakis, "Inducing passive nonlinear energy sinks in vibrating systems," *J. Vibrat. Acoust.*, vol. 123, no. 3, pp. 324–332, 2001.

[31] E. Gourdon and C. H. Lamarque, "Nonlinear energy sink with uncertain parameters," *J. Comput. Nonlinear Dyn.*, vol. 1, no. 3, pp. 187–195, 2006.

[32] X. Jiang, D. M. McFarland, L. A. Bergman, and A. F. Vakakis, "Steady state passive nonlinear energy pumping in coupled oscillators: Theoretical and experimental results," *Nonlinear Dyn.*, vol. 33, no. 1, pp. 87–102, 2003.

[33] A. F. Vakakis, L. Manevitch, O. Gendelman, and L. Bergman, "Dynamics of linear discrete systems connected to local, essentially non-linear attachments," *J. Sound Vibrat.*, vol. 264, no. 3, pp. 559–577, 2003.

[34] O. V. Gendelman and Y. Starosvetsky, "Quasi-periodic response regimes of linear oscillator coupled to nonlinear energy sink under periodic forcing," *J. Appl. Mech.*, vol. 74, no. 2, pp. 325–331, 2007.

[35] O. V. Gendelman, Y. Starosvetsky, and M. Feldman, "Attractors of harmonically forced linear oscillator with attached nonlinear energy sink I: Description of response regimes," *Nonlinear Dyn.*, vol. 51, nos. 1–2, pp. 31–46, 2008.

[36] Y. Starosvetsky and O. V. Gendelman, "Attractors of harmonically forced linear oscillator with attached nonlinear energy sink. II: Optimization of a nonlinear vibration absorber," *Nonlinear Dyn.*, vol. 51, nos. 1–2, pp. 47–57, 2008.

[37] O. Gendelman, L. I. Manevitch, A. F. Vakakis, and R. M'Closkey, "Energy pumping in nonlinear mechanical oscillators: Part I—Dynamics of the underlying Hamiltonian systems," *J. Appl. Mech.*, vol. 68, no. 1, pp. 34–41, 2001.

[38] O. V. Gendelman, "Transition of energy to a nonlinear localized mode in a highly asymmetric system of two oscillators," *Nonlinear Dyn.*, vol. 25, nos. 1–3, pp. 237–253, 2001.

[39] O. Gendelman and A. F. Vakakis, "Energy pumping in nonlinear mechanical oscillators: Part II—Resonance capture," *J. Appl. Mech.*, vol. 68, no. 1, pp. 42–48, 2000.

[40] O. M. Anubi, D. R. Patel, and C. D. Crane, III, "A new variable stiffness suspension system: Passive case," *Mech. Sci.*, vol. 4, no. 1, pp. 139–151, 2013. [Online]. Available: http://www.mech-sci.net/4/139/2013/

[41] J. Smoker, A. Baz, and L. Zheng, "Virtual reality simulation of active car suspension system," *Int. J. Virtual Reality*, vol. 8, no. 2, pp. 75–82, 2009.

[42] J. Schoukens, R. Pintelon, Y. Rolain, and T. Dobrowiecki, "Frequency response function measurements in the presence of nonlinear distortions," *Automatica*, vol. 37, no. 6, pp. 939–946, 2001.

[43] A. J. Stack and F. J. Doyle, "A measure for control relevant nonlinearity," in *Proc. Amer. Control Conf.*, Seattle, WA, USA, 1995, pp. 2200–2204.

[44] D. Karnopp, M. J. Crossby, and R. A. Harwood, "Vibration control using semi-active force generators," *J. Manuf. Sci. Eng.*, vol. 96, no. 2, pp. 619–626, 1974.

[45] H. Laalej, Z. Q. Lang, B. Sapinski, and P. Martynowicz, "MR damper based implementation of nonlinear damping for a pitch plane suspension system," *Smart Mater. Struct.*, vol. 21, no. 4, p. 045006, 2012.

[46] M. A. X. Song and S. C. Sotuhward, "Modeling magnetorheological dampers with application of nonparametric approach," *J. Intell. Mater. Syst. Struct.*, vol. 16, no. 5, pp. 421–432, 2005.

[47] E. Guglielmino, T. Sireteanu, C. W. Stammers, G. Ghita, and M. Giuclea, *Semi-Active Suspension Control: Improved Vehicle Ride and Road Friendliness*. New York, NY, USA: Springer-Verlag, 2008.

[48] Y. K. Wen and M. Asce, "Method for random vibration of hysteric systems," *J. Eng. Mech. Division*, vol. 102, nos. 1–3, pp. 249–263, 1976.

[49] I. H. Shames and F. A. Cozzarelli, *Elastic and Inelastic Stress Analysis*. New York, NY, USA: Taylor & Francis, 1997.

[50] S. Guo, S. Yang, and C. Pan, "Dynamic modeling of magnetorheological damper behaviors," *J. Intell. Mater. Syst. Struct.*, vol. 17, no. 1, pp. 3–14, 2006.

[51] J.-H. Koo, F. D. Goncalves, and M. Ahmadian, "A comprehensive analysis of the response time of MR dampers," *Smart Mater. Struct.*, vol. 15, no. 2, p. 351, 2006.

[52] H. Khalil and J. Grizzle, *Nonlinear Systems*, vol. 3. Englewood Cliffs, NJ, USA: Prentice-Hall, 1996.

[53] A. Zin, O. Sename, M. Basset, L. Dugard, and G. Gissinger, "A nonlinear vehicle bicycle model for suspension and handling control studies," in *Proc. IFAC Conf. Adv. Veh. Control Safety (AVCS)*, Genova, Italy, Oct. 2004, pp. 638–643.

Olugbenga Moses Anubi received the Ph.D. degree in mechanical engineering from the University of Florida, Gainesville, FL, USA, with a focus on variable stiffness suspension system.

He is currently a Post-Doctoral Researcher with the Hyundai Center of Excellence in Vehicle Dynamics Systems and Control, University of California at Davis, Davis, CA, USA. His current research interests include control theoretical development and applications, modeling of dynamical systems, vehicle system dynamics and control, soft computing, and robotics.

Carl Crane received the bachelor's and master's degrees in mechanical engineering from the Rensselaer Polytechnic Institute, Troy, NY, USA, and the Ph.D. degree from the University of Florida, Gainesville, FL, USA.

He is currently a Professor with the Department of Mechanical and Aerospace Engineering, University of Florida, and the Director of the Center for Intelligent Machines and Robotics. He has authored one book and over 40 papers in the areas of spatial geometry and robotic systems. He has researched spatial mechanisms, tensegrity systems, robotics, and autonomous navigation for over 25 years, and is currently developing system architectures for autonomous ground vehicle navigation and passive parallel mechanisms for force control applications.

Dr. Crane is a fellow of the American Society of Mechanical Engineers, and also spent five years as an Officer in the Army Corps of Engineers. He was the team leader of UFs 2004 and 2005 DARPA Grand Challenge autonomous vehicle development efforts and UFs 2007 DARPA Urban Challenge project team.